Electronic Supplementary Information

Inverse Heavy-Atom Effect in Near Infrared Photoluminescent Gold Nanoclusters

Goutam Pramanik, Klaudia Kvakova, Muhammed Arshad Thottappali, David Rais, Jiri Pfleger, Michael Greben, Ayman El-Zoka, Sara Bals, Martin Dracinsky, Jan Valenta*, and Petr Cigler*

Corresponding authors: P. Cigler (cigler@uochb.cas.cz), J. Valenta (jan.valenta@mff.cuni.cz)

Materials

All reagents were purchased from commercial sources and used as received. Aqueous solutions for all experiments were prepared using Milli-Q water.

Synthesis of AuNCs

Synthesis of 1

AuNC **1** was prepared by following our previously reported procedure.[1] Briefly, thioctic acid (1.3 mg, 6.3 μmol) was dissolved in 3.9 mL MilliQ water by adding 10 μL of 2 M NaOH. After 15 min of stirring, 1.7 μL of $HAuCl_4.3H_2O$ (470 mg/mL) was added. The reaction mixture was stirred at room temperature for an additional 15 min, 80 μL freshly prepared $NaBH_4$ solution (1.9 mg/mL) was added, and the reaction mixture was stirred overnight. The next day, the solution was purified by three cycles of centrifugation/filtration using a membrane filtration device with a molecular weight cut-off (MWCO) of 3 kDa. Then, thiol-terminated polyethylene glycol (MW 2000; 2.6 mg; 1.3 μmol) was added to the solution and the pH was adjusted to 7-7.5. The mixture was stirred overnight. The dispersion was purified by three cycles of centrifugation/filtration using a membrane filtration device with MWCO of 3 kDa.

Synthesis of 2

A solution of **1** (4 mL, 0.2 mg/mL) and benzylamine (BA) (2 μL, ~18.3 μmol) was prepared, and the pH was adjusted to the 4.5 – 6.0 range with 1 M HCl. The mixture was stirred for 15 min. Then, the reaction was initiated by adding excess *N*-(3-dimethylaminopropyl)-*N*′-ethylcarbodiimide hydrochloride (EDC.HCl) (10 mg, 52 μmol) and stirred overnight. The following day, the dispersion was purified by three cycles of centrifugation/filtration using a membrane filtration device with a MWCO of 3 kDa to obtain **2**.

Synthesis of 3

4-Iodobenzylamine.HCl (iBA) (9.8 mg, ~ 36.6 μmol) was added to a solution of **1** (4 mL, 0.2 mg/mL), and the pH was adjusted to the 4.5 – 6.0 range with 1 M HCl. The mixture was stirred until iBA completely dissolved (~20-30 min). The reaction was started by adding excess EDC.HCl (10 mg, 52 μmol) and was stirred for 2 h. After 2 h, the pH of the reaction mixture was adjusted to 4.5 – 6.0 with 1 M HCl and an additional 10 mg EDC.HCl was added. The addition of EDC.HCl was repeated once more after 2 h, and the reaction mixture was stirred overnight at room temperature. Excess iBA and EDC.HCl were added thrice because of the slow reactivity of iBA with **1** compared with BA. The dispersion was purified by three cycles of centrifugation/filtration using a membrane filtration device with a MWCO of 3 kDa to obtain **3**.

Characterization of AuNCs

Elemental Analysis

Au, S, and N content were estimated using an optical emission spectrometer (OES) with radial observation of inductively coupled plasma (ICP) (SPECTRO Arcos – SPECTRO Analytical Instruments, Kleve,

Germany). The determination of N in solid AuNC samples was performed using an automatic PE 2400 Series II CHNS/O Analyser.

Table S1: Combined data from inductively coupled plasma optical emission spectrometry (ICP-OES) and CHN analysis.

Sample Name	Au (weight %)	S (weight %)	N (weight %)	Au (mol %)	S (mol %)	N (mol %)	Au/S molar ratio	Au/N molar ratio
2	21.34	4.44	0.32	0.10	0.13	0.023	0.76	4.34
3	16.12	3.6	0.26	0.08	0.11	0.019	0.72	4.21

NMR Measurements

NMR spectra were measured on a Bruker Avance III 500 spectrometer (499.88 MHz for ^{1}H) equipped with a 5 mm PFG cryoprobe. All ^{1}H spectra were acquired for samples in D_2O and referenced to the solvent signal (4.8 ppm).

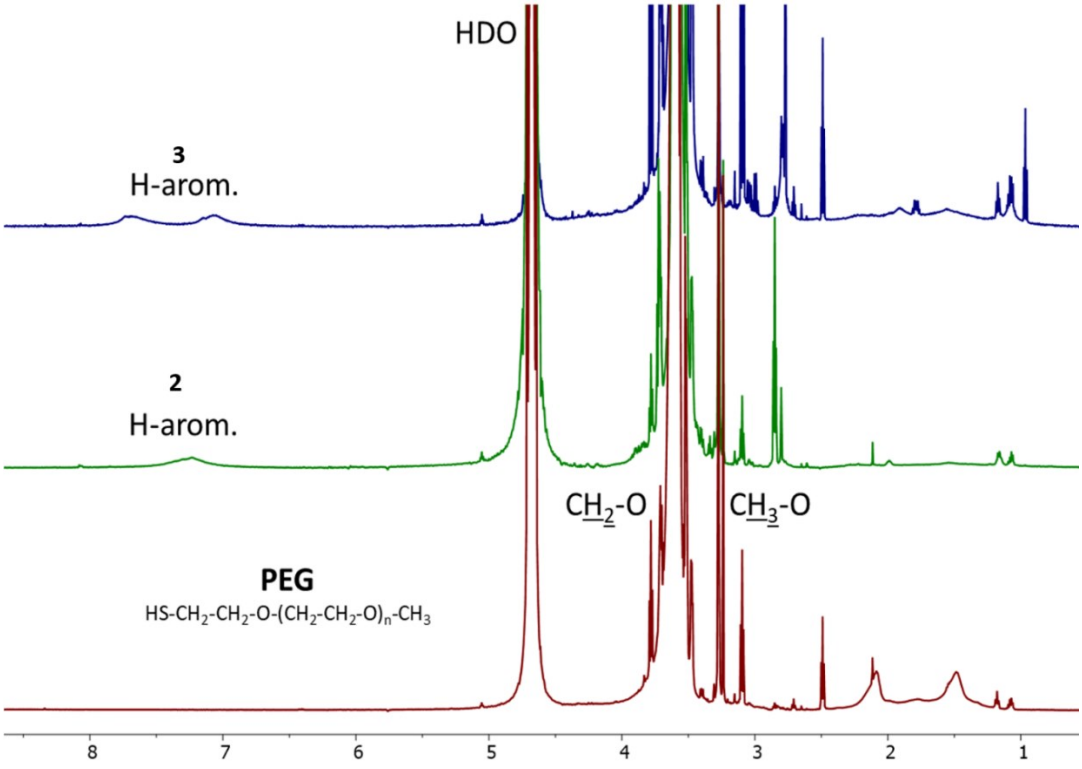

Figure S1: ^{1}H NMR (499.98 MHz, D_2O) of AuNC **2**, **3** and PEG. The peaks were referenced to the solvent signal.

Zeta potential measurements

Zeta potential experiments were carried out on a Zetasizer Nano ZSP (Malvern Instruments, Malvern, UK) with a 633 nm laser at 25 °C. Universal dip cells in disposable cuvettes were used. A 10-µL aliquot of AuNC solution (200 µg/mL) was mixed with 1 mL phosphate buffer solution (10 mM, pH 7.4) for measurement. Average values of at least three data points are reported.

High-resolution scanning transmission electron microscopy (HR-STEM) and X-ray photoelectron spectroscopy (XPS) measurements

The sizes of the AuNCs were determined by HR-STEM using an FEI Titan microscope. Samples were analyzed at a high voltage of 200 kV and a probe current of 50 pA.

XPS were measured using Omicron Nanotechnology equipment. The primary X-ray beam was monochrome radiation from an Al lamp with an energy of 1486.7 eV. The constant analyzer energy (CAE) mode was used, and the intensity calibration was based on copper and copper spectra-derived calibration constants. The ion gun used argon ions with an energy of ~5 keV; ion etching was carried out in the preparation chamber. A circular area with a diameter of approximately 0.8 mm was analyzed. The spectra were evaluated with CasaXPS software. The binding energy of a C 1s (284.8 eV) was used to calibrate the binding energy axis.

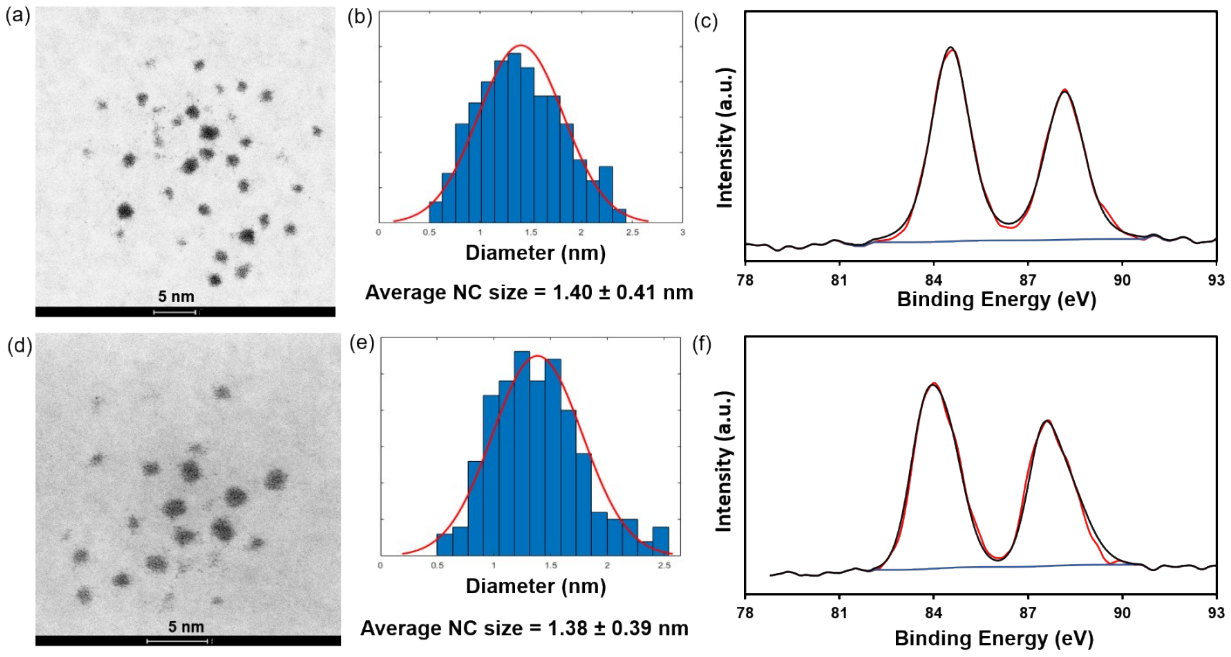

Figure S2: HR-STEM images of **2 (a)** and **3 (d)**. Particle size analysis of **2 (b)** and **3 (e)**. Particle size analysis of 200 AuNCs was performed for all samples. AuNCs were selected randomly from over 20 different locations in each sample. XPS spectra of the Au 4f peaks of **2 (c)** and **3 (f)**. The curves show that both AuNCs comprise Au(0) and Au(I).

UV-vis absorption and photoluminescence spectra, kinetics and yield measurements

UV-vis absorption spectra of aqueous solutions of AuNCs were measured with a Specord 250 spectrophotometer (Analytik Jena, Germany). Photoluminescence (PL) spectra were recorded under excitation by a cw 405-nm diode laser (MSL-III-405, CNI Co. Ltd., China) with acousto-optical modulation for time-resolved measurements and detected by an imaging spectrograph (SP 2300i, Acton, USA) with an LN-cooled CCD (Spec-10:400B, Princeton Instruments, USA) or (for time-resolved PL) a photon-counting photomultiplier (H11526–20-NF Hamamatsu, Japan) and multichannel scaler card (MSA-300, Becker & Hickl MSA-300, Germany).

As the excitation pulse sharpness (leading and trailing edges) produced by the AO modulator is approximately 100 ns, faster processes are not probed within these measurements, which can slightly affect the determined average decay time. However, in the case of significant presence of such processes, there should be an observable step down of PL signal at the end of the excitation pulse, which was not the case with our AuNCs.

PL decay kinetics were analyzed by three-exponential fitting:

$$I(t) = \sum_{i=1}^{3} A_i e^{-(\frac{t}{\tau_i})} + offset \qquad (1)$$

The PL quantum yield (Fig. S3) was measured with the same detection system (spectrometer and CCD) but excitation was performed using a laser-driven light source (LDLS, Energetiq, USA) coupled to a monochromator (SP 2150i, Acton, USA). Each sample was placed in a 10-cm diameter integrating sphere (Sphere Optics, Germany) with excitation and emission signals coupled via quartz fiber bundles (Newport, USA).

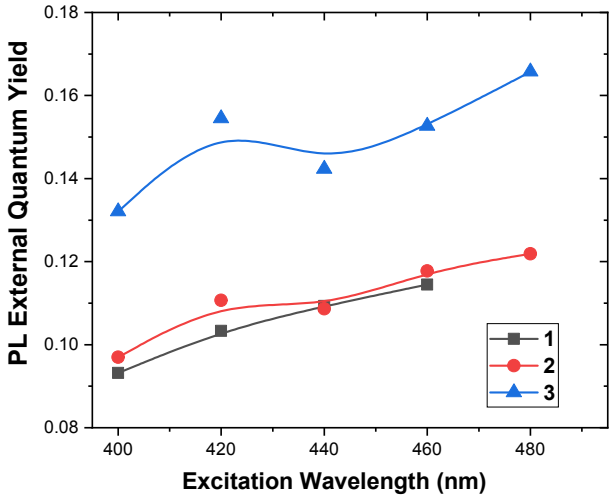

Figure S3: The external quantum yield of PL for excitation in the violet-blue-green spectral region. The PL QY uncertainty is about ±1%. The slight decrease of PL QY for excitation at short wavelengths may be due to increasing loses by absorption in ligands.

Transient Absorption measurements

Femtosecond transient absorption (fsTA) spectra were measured with ultrafast pump-probe experimental setup HELIOS (Ultrafast Systems, LLC, USA) using ultrafast laser source LEGEND ELITE (Coherent, USA) at 1 kHz repetition rate. The excitation pulses from TOPAS (Light Conversion, Lithuania) were adjusted to 360 nm and 260 nJ/pulse. The white-light continuum probe pulses were derived from the CaF_2 crystal. Laser pulses of both pump and probe beams were linearly polarized with mutual orientation of polarization at 55 deg. (magic angle) to suppress the rotational depolarization effect on the observed time evolution of the fsTA signal.

To observe the evolution of the transient absorption at the time scale longer than 6 ns (nsTA), the same source of probe light pulses was used as described above for fsTA. The pump pulses (wavelength 355 nm) were sourced from an electronically synchronized Nd-YAG laser (Surelite SL I-10, Continuum, USA) at the repetition rate 10 Hz, and frequency doubled using second harmonic generator and dichroic separator. The polarizations of the pump and probe pulses were also at the magic angle, as in the case of the fsTA.

TA spectra were measured with the sample colloids filled in 2 mm optical path quartz cuvettes under continuous stirring. For better understanding of the influence of atmospheric gases, the nsTA experiment was performed also with degassed samples in 10 mm optical path cuvettes equipped with a gas-tight valve.

Data analysis: Transient absorption datasets (both fsTA shown in Figure **S4** and nsTA in Figure **S5**) were analyzed using a global fitting approach. The spectro-temporal evolutions in femtosecond and picosecond time scale were well fitted with a sequential two-compartment kinetic model. The corresponding spectral profiles associated with the corresponding two-time constants sufficiently well fitted the observed transient spectra obtained from fsTA. However, since the lifetimes obtained from the fsTA experiment for the long-lifetime component markedly exceeded the maximum available delay time, we consider them not reliable and, hence, the long lifetimes shown in the main text of the paper were taken only from the nsTA experiment. Using global analysis, the data from the nsTA were relatively well fitted already with a single exponential kinetic model. Some wavelengths were, however, overestimated which lead to a sub-optimal fit for the wavelengths where the TA signal is more pronounced. Better agreement with experimental data was obtained when an additional component was added, with its life time much exceeding the experimental time scale (see table S2). For the sake of noise reduction, all spectral profiles shown in Fig. S5 were smoothed by adjacent averaging of 4-5 points.
In fsTA, no difference in the behavior of aerated and degassed colloids was observed. On the contrary, in longer delay times the difference was large, as seen from data obtained using nsTA (cf. Fig. S5c and S5d).

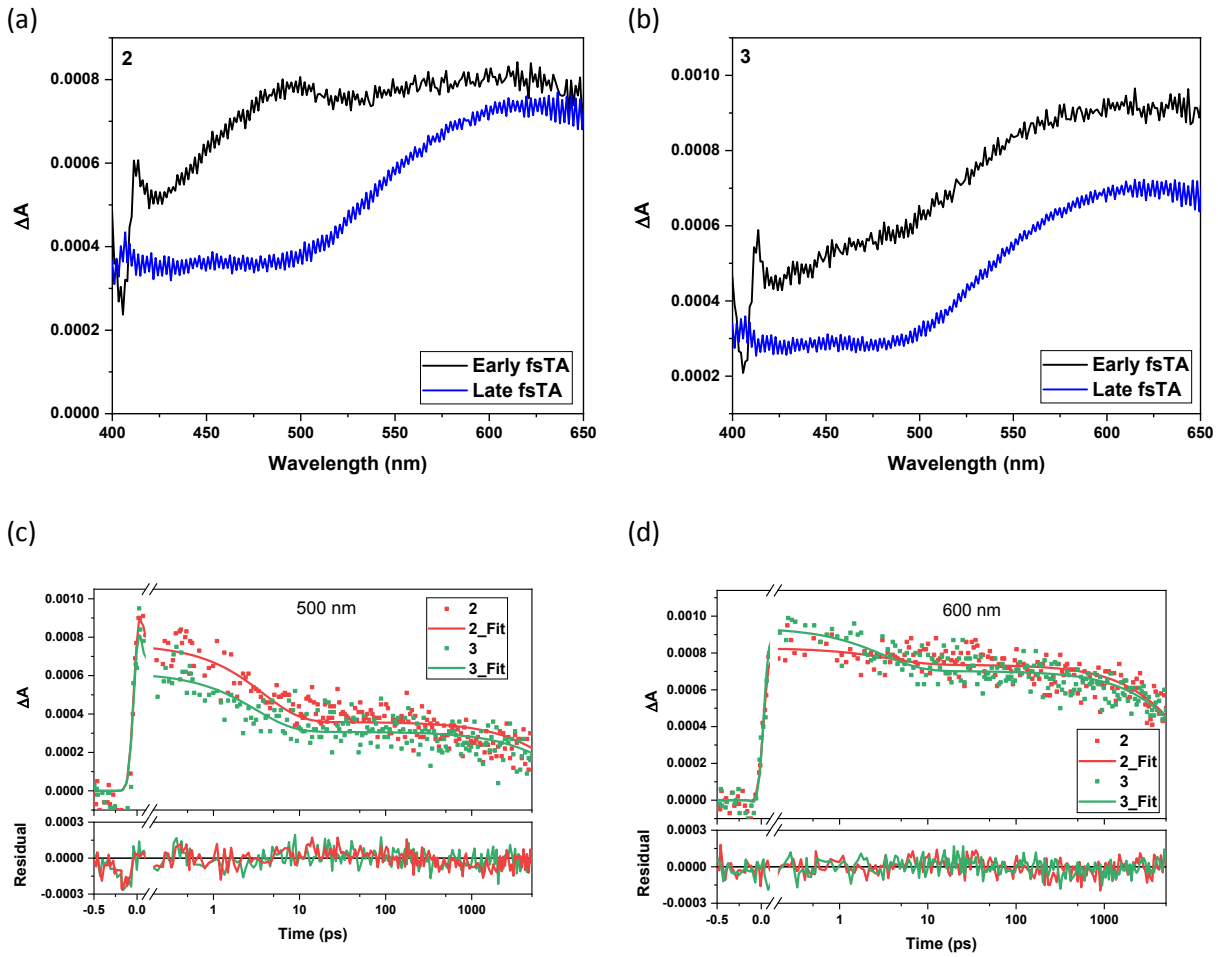

Figure S4: **a, b** – Short (black curves) and long (blue curves) transient absorption spectral components of colloids **2 (a)** and **3 (b)** as obtained from the global analysis of the fsTA measurements. **c, d** - temporal TA profiles obtained for probe wavelengths 500 nm **(c)** and 600 nm **(d)**, respectively. Excitation wavelength 360 nm in all cases. All colloids were aerated but no difference for the degassed colloids was observed.

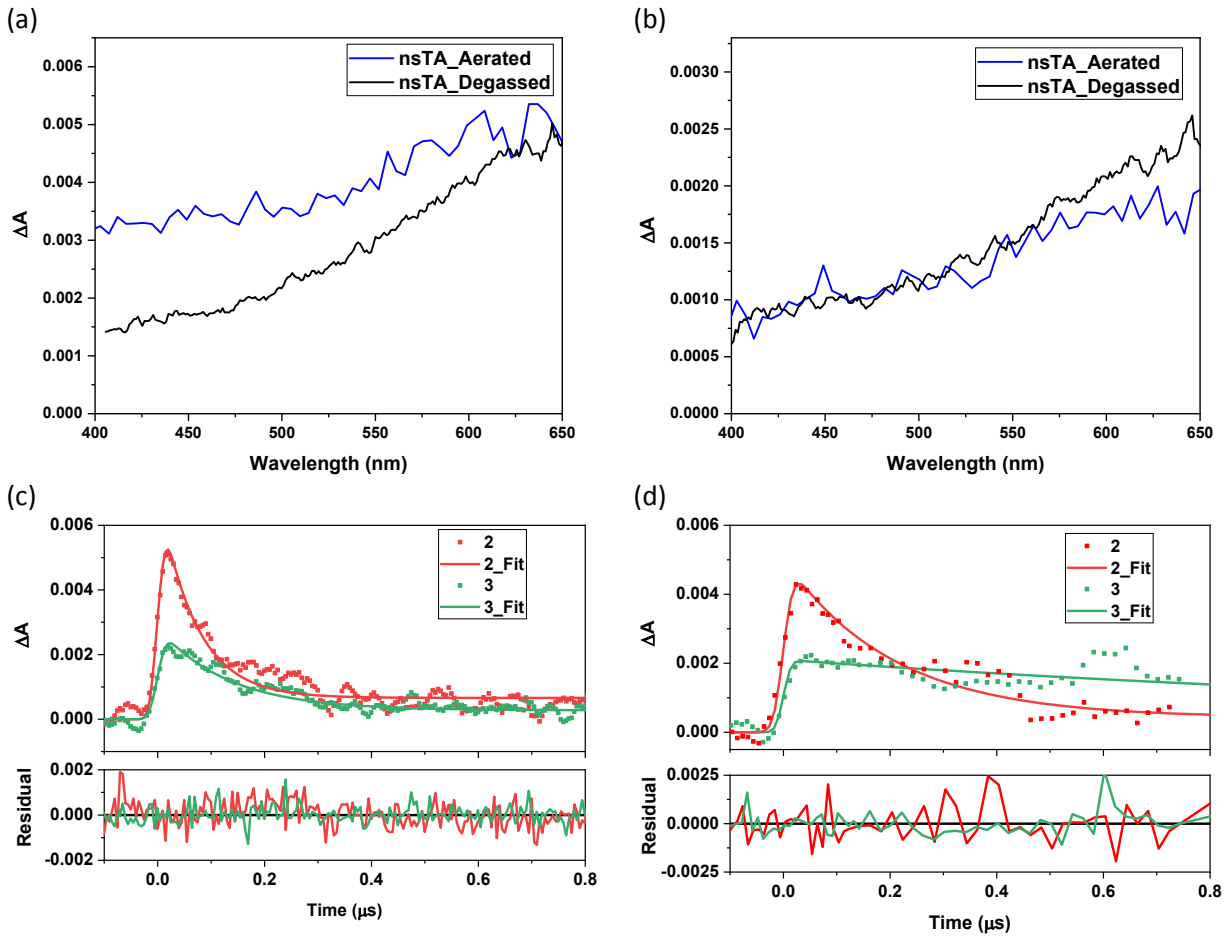

Figure S5: a, b - Transient absorption spectral components of aerated (blue curves) and degassed (black curves) colloids of samples **2 (a)** and **3 (b)**. **c, d** - kinetics of TA at the probe wavelength 600 nm measured with nsTA on aerated **(c)** and degassed **(d)** colloids of samples **2** (red) and **3** (green). Smooth curves show the fitted spectral and temporal profiles obtained from the global analysis. Excitation wavelength 355 nm in all cases.

Table S2: Lifetimes derived from individual spectral components.

Sample	fsTA	nsTA aerated					nsTA degassed				
		single exponential		bi-exponential kinetic model			single exponential		bi-exponential kinetic model		
	τ^{TA}_1 (ps)	τ^{TA}_2 (µs)	RMS value	τ^{TA}_2 (µs)	τ^{TA}_3 (µs)	RMS value	τ^{TA}_2 (µs)	RMS value	τ^{TA}_2 (µs)	τ^{TA}_3 (µs)	RMS value
2	3.78 ± 0.01	0.16 ± 0.01	0.00093	0.07 ± 0.01	>> 10	0.00086	0.39 ± 0.01	0.00095	0.28 ± 0.01	140 ± 16	0.00087
3	3.16 ± 0.07	0.34 ± 0.01	0.00060	0.13 ± 0.01	>> 10	0.00055	2.12 ± 0.03	0.00069	1.86 ± 0.03	>> 10	0.00067

*) Lifetimes $\tau >> 10$ µs are out of the time scale of nsTA experiment and could not be reliably determined. The RMS value as reported by Glotaran is the sum of squares of the errors divided by the number of degrees of freedom.

References:

1 G. Pramanik, J. Humpolickova, J. Valenta, P. Kundu, S. Bals, P. Bour, M. Dracinsky and P. Cigler, *Nanoscale*, 2018, **10**, 3792–3798.